Quantum oscillations of the two-dimensional hole gas at atomically flat diamond surfaces

Yamaguchi Takahide,[1] Hiroyuki Okazaki,[1] Keita Deguchi,[1,2] Shinya Uji,[1,2] Hiroyuki Takeya,[1] Yoshihiko Takano,[1,2]
Hidetoshi Tsuboi,[3] and Hiroshi Kawarada[3]

[1]*National Institute for Materials Science, Sengen, Tsukuba 305-0047, Japan*
[2]*University of Tsukuba, Tennodai, Tsukuba 305-8571, Japan*
[3]*Waseda University, Okubo, Shinjuku, Tokyo 169-8555, Japan*

Shubnikov–de Haas oscillations are observed in atomically flat hydrogen-terminated diamond surfaces with high-density hole carriers introduced by the electric field effect using an ionic liquid. The Shubnikov–de Haas oscillations depend only on the magnetic field component perpendicular to the diamond surface, thus providing evidence of two-dimensional Fermi surfaces. The effective masses estimated from the temperature dependence of the oscillations are close to the cyclotron effective masses of the valence band maxima in diamond. The estimated quantum scattering time is one order of magnitude longer than the transport scattering time and indicates that the carrier mobility is locally as high as several thousand cm^2/V s at low temperature.

I. INTRODUCTION

Diamond is an electrical insulator with many unique properties, such as a wide band gap, high intrinsic carrier mobilities, high thermal conductivity, and high break-down electric field. These properties make diamond attractive for electronic applications, particularly when charge carriers are introduced. However, inducing low electrical resistivity and a high-mobility metallic state in diamond has been a long-standing challenge. A metallic state can be induced by heavy boron doping [1], but the critical dopant concentration is 2–3 orders of magnitude larger than those for Ge and Si [2–5]. Due to the significant lattice disorder caused by such a large dopant concentration, the carrier mobility is too low [6] for quantum (Shubnikov–de Haas) oscillations to be observed. Unlike doped Ge and Si [7,8], Shubnikov–de Haas (SdH) oscillations have not been reported for doped diamond.

An alternative clean approach for introducing carriers in semiconductors is to use the electric field effect. Two-dimensional electron gas formed in a Si metal-oxide-semiconductor field-effect transistor (MOSFET) exhibits clear SdH oscillations, as well as the quantum Hall effect [9]. However, difficulties arise in diamond because an intense electric field is required to induce a metallic state, and therefore, a significantly reduced surface roughness is also important; Shubnikov–de Haas oscillations in Si MOSFETs have been observed even at a small sheet carrier density of $\approx 10^{11}$ cm^{-2} [10]. However, a field-induced metallic state in diamond requires a much larger carrier density of the order of 10^{13} cm^{-2}. We have recently observed metallic behavior in hydrogen-terminated diamond surfaces by introducing hole carriers of 4×10^{13} cm^{-2} [11] using the electric double-layer transistor technique, capable of inducing an intense electric field on the channel surface [12–14]. Such high density hole carriers are expected to be confined within ≈ 1–2 nm below the diamond surface due to a strong electric field [15–18]. The carrier transport should therefore be affected by the surface roughness, typically 0.5 nm (root-mean-square value for a 1 μm^2 area) on polished diamond; reduced surface roughness is important to improve the transport properties.

The observation of Shubnikov–de Haas oscillations in diamond which we report in this paper was achieved by the preparation of atomically flat hydrogen-terminated diamond surfaces and the accumulation of high density hole carriers by the electric double-layer transistor technique. The Shubnikov–de Haas oscillations depend only on the magnetic field component perpendicular to the diamond surface, thus providing evidence of two-dimensional Fermi surfaces. From the temperature and magnetic field dependence of the oscillations, we also estimated the effective mass and quantum scattering time of the hole carriers. The estimated quantum scattering time indicates that the carrier mobility is locally as high as several thousand cm^2/V s at low temperature. The high-mobility two-dimensional metallic state in diamond demonstrated here will provide a rich field of research from fundamental physics to device applications that utilize the unique properties of diamond.

II. EXPERIMENTAL METHOD

We prepared an atomically flat diamond surface with steps and terraces using microwave plasma chemical vapor deposition (CVD) with an extremely low CH$_4$/H$_2$ ratio [19]: Mesas with a lateral dimension of 20×20–40×40 μm^2 and a height of ≈ 2 μm were fabricated using a photolithography and O$_2$ plasma etching on IIa (111) single-crystal diamond substrates with mechanically polished surfaces. After microwave plasma CVD on the substrates with a CH$_4$/H$_2$ ratio of 0.05% for 12 h, the surfaces of the mesas were inspected using an atomic force microscope. The top surface of some of the mesas was found to be atomically flat with triangular terraces [Fig. 1(a)]. The step height is approximately 0.21 nm, which corresponds to the bi-atomic layer height of the (111) diamond surface. As a result of the hydrogen plasma irradiation during the CVD, the diamond surface is hydrogen terminated. The hydrogen termination is considered to raise the energy bands of diamond relative to the vacuum level, thus favoring the introduction of hole carriers [15–17,20,21]. (The surface conductivity due to the hole carriers of the hydrogen-terminated diamond has been extensively studied from the viewpoint of both fundamental physics [15–17,20–25] and practical applications such as high-frequency field-effect transistors [25] and chemical and bio-sensors [26,27].)
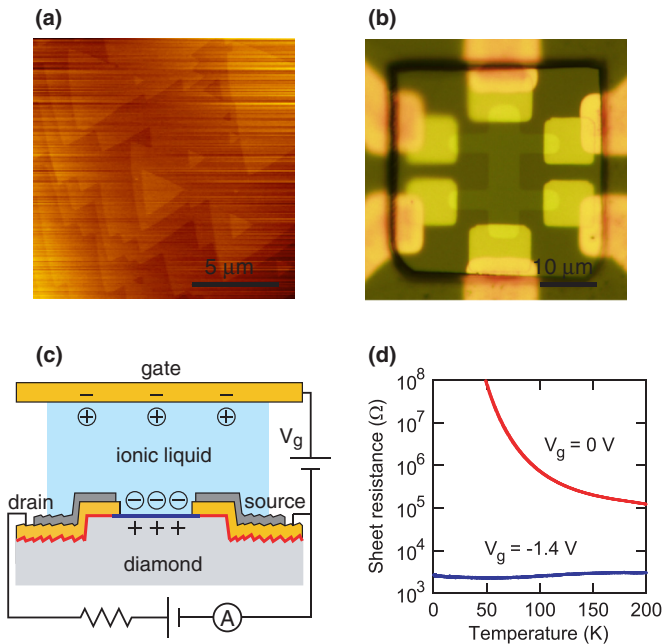
FIG. 1. (Color online) (a) Atomic force microscope image of an atomically flat (111) diamond surface with steps and terraces. This is the central part of the device shown in Fig. 1(b). (b) Hall bar on the top surface of a mesa with a lateral dimension of $\approx 40 \times 40$ μm; the top surface of the mesa is atomically flat as shown in Fig. 1(a). The surface of the Hall bar, which is used as the channel of an ionic liquid-gate transistor, is hydrogen terminated. The area other than the Hall bar is covered with Al_2O_3 for insulation. (c) Schematic diagram of the whole device. The blue line represents the hydrogen-terminated diamond surface, while the red line represents the oxygen-terminated diamond surface. A small amount of ionic liquid is applied between the diamond surface and gate electrode. (d) Temperature dependence of the sheet resistance of the device channel at $V_g = 0$ and -1.4 V.

We then fabricated a hall bar [Fig. 1(b)], used as the channel of an electric double-layer transistor, on such a flat surface using photolithography. A standard photolithography process is as follows: First, the hydrogen-terminated diamond surface was converted into an oxygen-terminated surface, except for the channel region of the device, using UV ozone treatment [28]. Pd with a thickness of 30 nm was then deposited to produce electrical contacts to the channel. Electrical leads to bonding pads were produced by the deposition of Au (210–300 nm)/Ti (35–50 nm). Finally, the area except the channel and bonding pads was covered by Al_2O_3 with a thickness of ≈ 30 nm. A small amount of ionic liquid, N,N-diethyl-N-methyl-N-(2-methoxyethyl) ammonium tetrafluoroborate (DEME-BF$_4$), was applied between the channel and top gate electrode [Fig. 1(c)].

The devices were set in a custom-built cryostat probe, which was then inserted in a physical property measurement system (Quantum Design) or a ^{3}He cryostat equipped with a superconducting magnet. The device was cooled down after the gate voltage was applied at a temperature $T \approx 260$ K. The temperature dependence of resistance [Fig. 1(d)] was measured using current and voltage preamplifiers with a dc bias of ± 50 mV to a series circuit of 10 MΩ and the device. The magnetic field dependence of resistance (Figs. 2–4) was
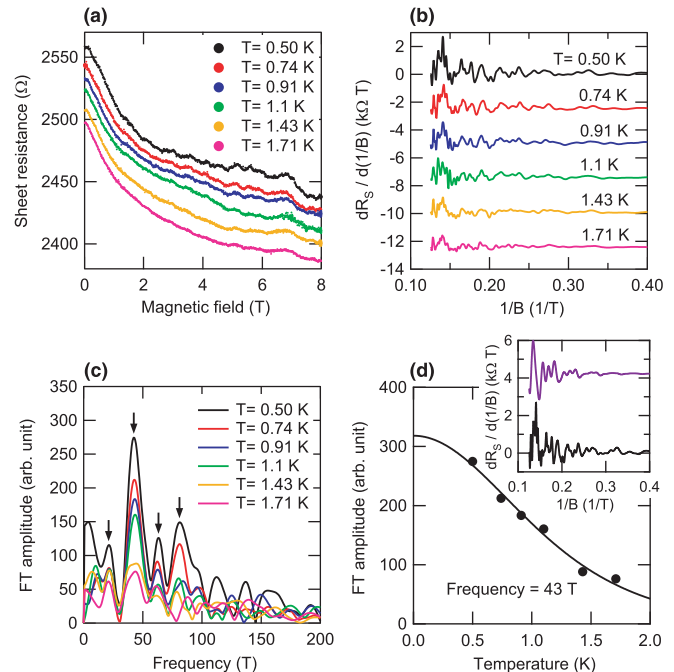

FIG. 2. (Color online) (a) Magnetic field (B) dependence of the sheet resistance R_s measured for $V_g = -1.4$ V at $T = 0.50$–1.71 K by applying a magnetic field perpendicular to the diamond surface. (b) Plot of $dR_s/d(1/B)$ as a function of $1/B$. The curves except for $T = 0.50$ K are offset vertically for clarity. (c) The Fourier spectra of the oscillations shown in Fig. 2(b) in the range $1/B = 0.125$–0.3 (1/T). Arrows indicate peaks at $F = 21, 43, 63,$ and 81 T. (d) Plot of the peak intensity at $F = 43$ T of the Fourier spectra [Fig. 2(c)] as a function of temperature. The fit yields the effective mass $m^*/m_0 = 0.66 \pm 0.03$. Inset: The bottom curve is $dR_s/d(1/B)$ as a function of $1/B$ at $T = 0.50$ K, which is the same as that shown in (b). The top curve was constructed as the sum of the oscillations for $F = 21, 43, 63,$ and 81 T calculated using Eq. (1) to provide a fit to the bottom curve, which determined a Dingle temperature of 1.8 K.

measured using a low-frequency (21, 29, or 71 Hz) lock-in technique with an ac current of 10 or 50 nA.

III. RESULTS AND DISCUSSION

The temperature dependences of the channel resistance of this device at $V_g = 0$ and -1.4 V are shown in Fig. 1(d). The diamond surface exhibits insulating behavior at $V_g = 0$ V [29]. As a negative voltage is applied to the gate, the sheet resistance decreases because the hole carriers are introduced. Details of the gate voltage dependence of Hall carrier density and mobility for similar devices have been reported elsewhere [11]. At $V_g = -1.4$ V, the sheet resistance decreases with decreasing temperature down to ≈ 50 K, indicating metallic carrier transport, although the resistance increases at lower temperature, suggesting weak localization. The Hall sheet carrier density and Hall mobility for $V_g = -1.4$ V measured at $T = 1.7$ K are, respectively, $n_{Hall} = 2.7 \times 10^{13}$ cm^{-2} and $\mu_{Hall} = 91$ cm^2/V s.

We observed SdH oscillations for a diamond surface with the high carrier density described above. Figure 2(a) shows the
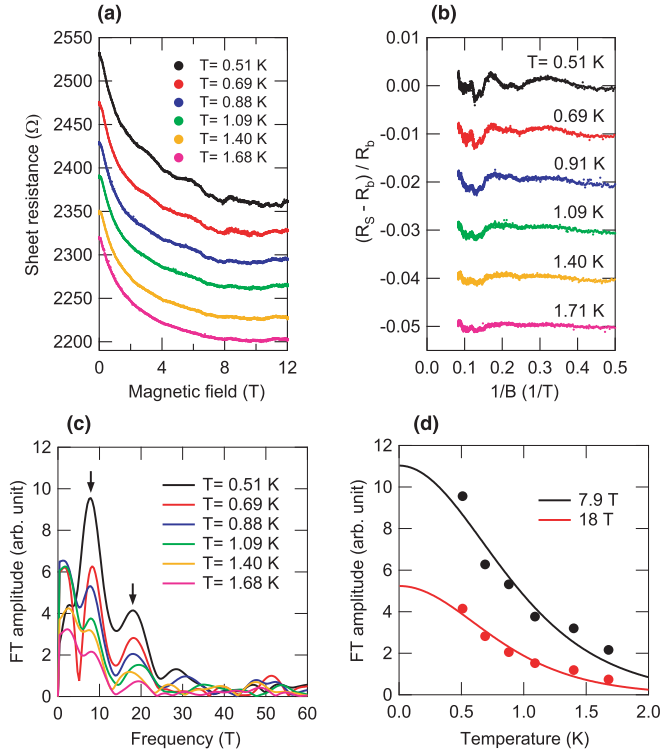
FIG. 3. (Color online) (a) Magnetic field (B) dependence of the sheet resistance R_s of another device measured for $V_g = -4$ V at $T = 0.51$–1.68 K by applying a magnetic field perpendicular to the (111) diamond surface. We note that this device was fabricated with a different lithography process from those described in Sec. II. For example, electrical contacts to the channel were made with TiC, which was produced by the deposition and annealing of Ti. Hall and resistance measurements lead to $n_{Hall} = 4.8 \times 10^{13}$ cm^{-2} and $\mu_{Hall} = 52$ cm^2/V s at $T = 0.50$ K. (b) Plot of the oscillatory component of the magnetoresistance as a function of $1/B$. The curves except for $T = 0.51$ K are offset vertically for clarity. (c) The Fourier spectra of the oscillations shown in (b) in the range $1/B = 0.833$–0.4 (1/T). Arrows indicate peaks at $F = 7.9$ and 18 T. (d) Plot of the peak intensity at $F = 7.9$ and 18 T of the Fourier spectra (c) as a function of temperature. The fits yield the effective mass $m^*/m_0 = 0.68 \pm 0.08$ (7.9 T) and 0.77 ± 0.08 (18 T).

magnetic field dependence of sheet resistance for $V_g = -1.4$ V, measured at $T = 0.50$–1.71 K by applying a magnetic field perpendicular to the surface. Oscillatory components are superimposed on the background of a negative magnetoresistance, with the amplitude decreasing with increasing temperature. To make the oscillations clearer, the derivative of the sheet resistance with respect to $1/B$ is numerically obtained and plotted as a function of $1/B$ in Fig. 2(b). The Fourier spectra of these oscillations in Fig. 2(b) in the range $1/B = 0.125$–0.3 (1/T) are shown in Fig. 2(c). Several peaks are visible; in particular, peaks at frequencies $F = 21, 43, 63$, and 81 T are evident in the Fourier spectra for different temperatures. The cross-sectional area A_F of the Fermi surface perpendicular to the magnetic field can be obtained from the frequency F of the SdH oscillation using the equation $F = (\phi_0/2\pi^2)A_F$, where $\phi_0 \equiv h/2e$ is the magnetic flux quantum. Using this formula, the area A_F for the four peaks are calculated as $0.20, 0.41, 0.61, 0.78$ nm^{-2},

which are $0.028\%, 0.057\%, 0.084\%$, and 0.11% of the (111) two-dimensional Brillouin zone. Taking spin degeneracy into account and using $n_{SdH} = A_F/(2\pi^2) = F/\phi_0$, these areas lead to the sheet carrier densities n_{SdH} of $1.1 \times 10^{12}, 2.2 \times 10^{12}, 3.2 \times 10^{12}$, and 4.1×10^{12} cm^{-2}. The sum of these sheet carrier densities n_{SdH} is smaller than the Hall sheet carrier density n_{Hall}. Similar discrepancies between n_{SdH} and n_{Hall} have been reported in recent studies of SdH oscillations in a Nb-doped SrTiO$_3$ thin film [30] and LaAlO$_3$/SrTiO$_{3-\delta}$ interfaces [31]. These discrepancies could be due to the existence of Fermi surfaces with a large effective mass and/or a small scattering time, the SdH oscillations of which cannot be observed in the temperature and magnetic field ranges of these measurements. Another possibility is that the carrier density and scattering time might be spatially inhomogeneous, particularly in our devices, due to the distortion that could be induced in the ionic liquid during the cooling process. The SdH signals may arise from small areas where the carrier density is lower and the scattering time is longer than in the major part of the channel. This picture is consistent with the small amplitude of the oscillations that we observe.

The resistance oscillation as a function of the magnetic field can be described by the equation [9]

$$\Delta R \propto -\frac{Kp\mu^*T/B}{\sinh(Kp\mu^*T/B)}\exp(-Kp\mu^*T_D/B)$$
$$\times \cos[2\pi p(F/B - 1/2)], \qquad (1)$$

where p indicates the pth harmonic, $\mu^* \equiv m^*/m_0$ (m^* and m_0 are the effective and free electron masses), $K \equiv 2\pi^2 k_B m_0/(\hbar e) \approx 14.7$ (T/K), $T_D \equiv \hbar/(2\pi k_B \tau_D)$ is the Dingle temperature, and τ_D is the carrier scattering time. By fitting the experimental data with this equation, the effective mass and scattering time of the carriers can be estimated. Figure 2(d) shows the peak intensity at $F = 43$ T of the Fourier spectra as a function of temperature. The fit to the temperature reduction factor
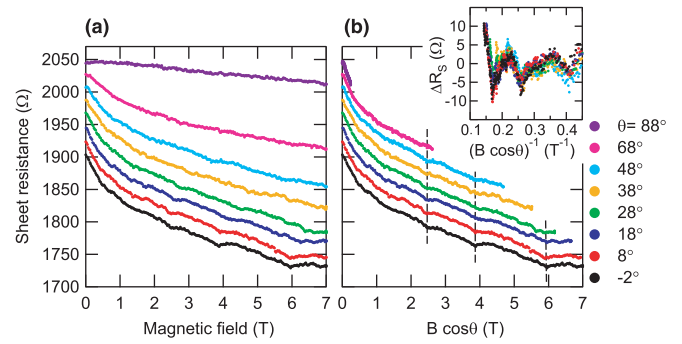

FIG. 4. (Color online) (a) Magnetic field dependence of resistance of a device (that is different from those shown in Figs. 2 and 3) measured for $V_g = -1.8$ V at 2.0 K for different magnetic field orientations. The field is perpendicular to the (111) diamond surface at $\theta = 0°$ and parallel to it at $\theta = 90°$. The curves except for $\theta = -2°$ are offset vertically for clarity. Hall and resistance measurements lead to $n_{Hall} = 5.7 \times 10^{13}$ cm^{-2} and $\mu_{Hall} = 52$ cm^2/V s at $T = 2.0$ K. (b) The same data in Fig. 4(a) plotted as a function of $B\cos\theta$. The curves except for $\theta = -2°$ are offset vertically for clarity. The dashed lines are a guide to the eye. The inset shows the oscillatory components of the curves shown in Fig. 4(a) as a function of $1/B\cos\theta$.

$(Kp\mu^*T/B)/\sinh(Kp\mu^*T/B)$ in Eq. (1) assuming $p = 1$ and $B = 2/(0.125 + 0.3) = 4.71$ T leads to the effective mass $m^*/m_0 = 0.66 \pm 0.03$. The effective masses for the other frequencies are obtained by similar fits: $m^*/m_0 = 0.36 \pm 0.07$, 0.63 ± 0.07, and 0.78 ± 0.11 for $F = 21, 63$, and 81 T. We have measured four devices with atomically flat diamond surfaces, all of which exhibited SdH oscillations. The number of clear peaks in Fourier spectra is different from device to device and at different gate voltages; see Fig. 3 for SdH oscillations observed in another device. However, the estimated effective mass for each peak is in the range $m^*/m_0 = 0.17$–0.36 (six peaks) or 0.57–0.78 (six peaks). The cyclotron effective masses of the valence band maxima (light-hole, split-off, and heavy-hole) in diamond for the magnetic field perpendicular to the (111) surface are $m^*/m_0 = 0.276$, 0.394, and 0.690 from a theoretical calculation [32,33], or 0.255, 0.375, and 0.702 from a recent experiment of cyclotron resonances [34]. Therefore, the above result indicates that the SdH oscillations arise from holes introduced into the valence bands of diamond.

The electronic states of the holes accumulated in the diamond surface should be quantized in the direction perpendicular to the surface, leading to subbands. A self-consistent solution of the Schrödinger equation and Poisson equation [15,16] shows that the first subbands of the light-hole, heavy-hole, and split-off bands are occupied in the carrier density range 3×10^{13}–6×10^{13} cm^{-2} of our devices. This prediction for an ideal diamond surface appears inconsistent with our observation that the effective masses for $F = 43$, 63, and 81 T for the device shown in Fig. 2 are close to the cyclotron effective mass for the heavy-hole band. The spatial inhomogeneity in the carrier density, described above, may yield these three frequencies; namely, they may arise from spatially different areas with different carrier densities. The Dingle temperatures for $F = 21, 43, 63$, and 81 T are obtained as 1.8 ± 0.3 K [see the inset of Fig. 2(d)]. This value corresponds to a quantum scattering time $\tau_D = (7 \pm 1) \times 10^{-13}$ sec. Meanwhile, the scattering time obtained from the Hall mobility and $m^*/m_0 = 0.66$ for $F = 43$ T is $\tau_{\text{Hall}} = 3.4 \times 10^{-14}$ sec, which is one order of magnitude shorter than τ_D. τ_{Hall} is generally longer than τ_D if they are associated with the same carrier component, because large-angle scattering mainly contributes to τ_{Hall}. The opposite result for our device is, however, again consistent with the idea that the SdH signals arise from small areas where the scattering time is longer than that of the major part of the channel. Thus, the present experimental results indicate that the carrier mobility is locally as high as $e\tau_D/m^* = 1500$–3300 cm^2/V s at $T = 0.5$ K. We consider that the Hall mobility could also be further increased by improving the device structure and fabrication process.

We now turn to the dependence of the SdH oscillation on the magnetic field orientation, from which the dimensionality of the Fermi surface can be examined. Figure 4(a) shows the magnetic field dependence of resistance of another device measured at 2.0 K for different field orientations. The field is perpendicular to the (111) diamond surface at $\theta = 0°$ and parallel to it at $\theta = 90°$. The negative magnetoresistance disappears as θ approaches $90°$, which also indicates two-dimensional weak localization. In addition, the nodes of the SdH oscillations shift to higher magnetic field as θ increases. The same data are plotted as a function of $B \cos\theta$ in Fig. 4(b). The oscillatory components are plotted as a function of $1/B \cos\theta$ in the inset. These figures show that the oscillations depend only on the magnetic field component perpendicular to the diamond surface, thus providing evidence of two-dimensional Fermi surfaces. We note that electron field emission measurements [35] and scanning tunneling spectroscopy [36,37] on hydrogen-terminated diamond surfaces (not atomically flat) indicate the presence of discrete quantized energy levels, but it is difficult to unambiguously determine the dimensionality of the electronic states in these measurements. In contrast, our observation that the SdH oscillations depend on $B \cos\theta$ clearly proves existence of two-dimensional electronic states on the atomically flat diamond surface.

IV. CONCLUSION

We observe Shubnikov–de Haas oscillations in atomically flat hydrogen-terminated diamond surfaces with high-density hole carriers introduced by the electric field effect using an ionic liquid. The analysis of the oscillations indicates that the estimated effective masses are close to the cyclotron effective masses of the valence band maxima in diamond. It also suggests that the carrier density and mobility are spatially inhomogeneous; the carrier mobility is locally as high as several thousand cm^2/V s at low temperature. Furthermore, the Shubnikov–de Haas oscillations depend only on the magnetic field component perpendicular to the diamond surface, thus providing evidence of two-dimensional Fermi surfaces. The high-mobility two-dimensional metallic state in diamond we demonstrated here will provide a rich field of research from low-temperature physics to device applications. Our results suggest that the mobility can be further improved, which may lead to the observation of quantum Hall effect [9] or superconductivity [38] in the two-dimensional hole gas in diamond. The combination of the metallic state with electron spins (with a long coherence time) or with optics (that are compatible with the ionic liquid gating) is also promising.

Note added in proof: After the submission of this paper, a report [39] appeared which claims the two-dimensionality of the surface conductivity of hydrogen-terminated diamond on the basis of the characteristics of in-plane-gate transistors (see also [40]).

[1] T. Yokoya, T. Nakamura, T. Matsushita, T. Muro, Y. Takano, M. Nagao, T. Takenouchi, H. Kawarada, and T. Oguchi, Nature (London) **438**, 647 (2005).

[2] T. Klein, P. Achatz, J. Kacmarcik, C. Marcenat, F. Gustafsson, J. Marcus, E. Bustarret, J. Pernot, F. Omnes, Bo E. Sernelius, C. Persson, A. Ferreirada Silva, and C. Cytermann, Phys. Rev. B **75**, 165313 (2007).

[3] A. Kawano, H. Ishiwata, S. Iriyama, R. Okada, T. Yamaguchi, Y. Takano, and H. Kawarada, Phys. Rev. B **82**, 085318 (2010).

[4] K. M. Itoh, E. E. Haller, J. W. Beeman, W. L. Hansen, J. Emes, L. A. Reichertz, E. Kreysa, T. Shutt, A. Cummings, W. Stockwell, B. Sadoulet, J. Muto, J. W. Farmer, and V. I. Ozhogin, Phys. Rev. Lett. **77**, 4058 (1996).

[5] P. Dai, Y. Zhang, and M. P. Sarachik, Phys. Rev. B **45**, 3984 (1992).

[6] For example, the mobility of boron-doped metallic diamond with a carrier density $n = 3 \times 10^{20}$–8×10^{21} cm^{-3} is 0.8–3 cm^2/V s; T. H. Borst and O. Weis, Phys. Status Solidi A **154**, 423 (1996); K. Ishizaka, R. Eguchi, S. Tsuda, T. Yokoya, A. Chainani, T. Kiss, T. Shimojima, T. Togashi, S. Watanabe, C.-T. Chen, C. Q. Zhang, Y. Takano, M. Nagao, I. Sakaguchi, T. Takenouchi, H. Kawarada, and S. Shin, Phys. Rev. Lett. **98**, 047003 (2007).

[7] W. Bernard, H. Roth, W. D. Straub, and J. E. Mulhern, Jr., Phys. Rev. **135**, A1386 (1964).

[8] W. D. Straub, H. Both, W. Bernard, S. Goldstein, and J. E. Mulhern, Jr., Phys. Rev. Lett. **21**, 752 (1968).

[9] T. Ando, A. B. Fowler, and F. Stern, Rev. Mod. Phys. **54**, 437 (1982).

[10] S. V. Kravchenko, A. A. Shashkin, D. A. Bloore, and T. M. Klapwijk, Solid State Commun. **116**, 495 (2000).

[11] T. Yamaguchi, E. Watanabe, H. Osato, D. Tsuya, K. Deguchi, T. Watanabe, H. Takeya, Y. Takano, S. Kurihara, and H. Kawarada, J. Phys. Soc. Jpn. **82**, 074718 (2013).

[12] K. Ueno, S. Nakamura, H. Shimotani, A. Ohtomo, N. Kimura, T. Nojima, H. Aoki, Y. Iwasa, and M. Kawasaki, Nat. Mater. **7**, 855 (2008)

[13] A. T. Bollinger, G. Dubuis, J. Yoon, D. Pavuna, J. Misewich, and I. Božović, Nature (London) **472**, 458 (2011).

[14] J. T. Ye, Y. J. Zhang, R. Akashi, M. S. Bahramy, R. Arita, and Y. Iwasa, Science **338**, 1193 (2012).

[15] C. E. Nebel, B. Rezek, and A. Zrenner, Diamond Relat. Mater. **13**, 2031 (2004).

[16] M. T. Edmonds, C. I. Pakes, and L. Ley, Phys. Rev. B **81**, 085314 (2010).

[17] M. Dankerl, A. Lippert, S. Birner, E. U. Stützel, M. Stutzmann, and J. A. Garrido, Phys. Rev. Lett. **106**, 196103 (2011).

[18] K. Nakamura, S. H. Rhim, A. Sugiyama, K. Sano, T. Akiyama, T. Ito, M. Weinert, and A. J. Freeman, Phys. Rev. B **87**, 214506 (2013).

[19] N. Tokuda, H. Umezawa, H. Kato, M. Ogura, S. Gonda, K. Yamabe, H. Okushi, and S. Yamasaki, Appl. Phys. Express **2**, 055001 (2009).

[20] F. Maier, M. Riedel, B. Mantel, J. Ristein, and L. Ley, Phys. Rev. Lett. **85**, 3472 (2000).

[21] C. E. Nebel, F. Ertl, C. Sauerer, M. Stutzmann, C. F. O. Graeff, P. Bergonzo, O. A. Williams, and R. B. Jackman, Diamond Relat. Mater. **11**, 351 (2002).

[22] M. I. Landstrass and K. V. Ravi, Appl. Phys. Lett. **55**, 975 (1989).

[23] H. Kawarada, Surf. Sci. Rep. **26**, 205 (1996).

[24] Ri Sung Gi, K. Tashiro, S. Tanaka, T. Fujisawa, H. Kimura, T. Kurosu, and M. Iida, Jpn. J. Appl. Phys. **38**, 3492 (1999).

[25] K. Hirama, H. Takayanagi, S. Yamauchi, J. H. Yang, H. Kawarada, and H. Umezawa, Appl. Phys. Lett. **92**, 112107 (2008).

[26] M. Dankerl, S. Eick, B. Hofmann, M. Hauf, S. Ingebrandt, A. Offenhäusser, M. Stutzmann, and J. A. Garrido, Adv. Funct. Mater. **19**, 2915 (2009).

[27] H. Kawarada and A. R. Ruslinda, Phys. Status Solidi A **208**, 2005 (2011).

[28] T. Sakai, K.-S. Song, H. Kanazawa, Y. Nakamura, H. Umezawa, M. Tachiki, and H. Kawarada, Diamond Relat. Mater. **12**, 1971 (2003).

[29] The CVD diamonds used in this study contain boron of 1×10^{19} cm^{-3} (from secondary ion mass spectrometry) because of an unintentional inclusion from remnants in the CVD chamber. Lower sheet resistance at $V_g = 0$ in Fig. 1(d) than in Fig. 5(a) of Ref. [11] is due to the carriers from the boron impurities. (The boron concentration of the sample in Fig. 5(a) of Ref. [11] is 3×10^{17} cm^{-3}.) As shown in Fig. 1(d), however, the conductivity due to the carriers from the boron impurities at $V_g = 0$ is negligibly small at ≈ 1 K.

[30] Y. Kozuka, M. Kim, C. Bell, B. G. Kim, Y. Hikita, and H. Y. Hwang, Nature (London) **462**, 487 (2009).

[31] A. D. Caviglia, S. Gariglio, C. Cancellieri, B. Sacépé, A. Fête, N. Reyren, M. Gabay, A. F. Morpurgo, and J.-M. Triscone, Phys. Rev. Lett. **105**, 236802 (2010).

[32] M. Willatzen, M. Cardona, and N. E. Christensen, Phys. Rev. B **50**, 18054 (1994).

[33] G. Dresselhaus, A. F. Kip, and C. Kittel, Phys. Rev. **98**, 368 (1955).

[34] N. Naka, K. Fukai, Y. Handa, and I. Akimoto, Phys. Rev. B **88**, 035205 (2013).

[35] L. Gan, E. Baskin, C. Saguy, and R. Kalish, Phys. Rev. Lett. **96**, 196808 (2006).

[36] C. E. Nebel, N. Yang, H. Uetsuka, T. Yamada, and H. Watanabe, J. Appl. Phys. **103**, 013712 (2008).

[37] A. Bolker, C. Saguy, M. Tordjman, L. Gan, and R. Kalish, Phys. Rev. B **83**, 155434 (2011).

[38] P. Phillips, Y. Wan, I. Martin, S. Knysh, and D. Dalidovich, Nature (London) **395**, 253 (1998).

[39] M. V. Hauf, P. Simon, M. Seifert, A. W. Holleitner, M. Stutzmann, and J. A. Garrido, Phys. Rev. B **89**, 115426 (2014).

[40] M. Tachiki, H. Seo, T. Banno, Y. Sumikawa, H. Umezawa, and H. Kawarada, Appl. Phys. Lett. **81**, 2854 (2002).